Title
Effect of welding sequence on welding-induced-alignment-distortion in packaging of butterfly laser diode modules: Simulation and experiment

Journal
Journal of Lightwave Technology, 23(2)

ISSN
0733-8724

Authors
Lin, Y M
Eichele, C
Shi, F G

Publication Date
2005-02-01

Peer reviewed

Effect of Welding Sequence on Welding-Induced-Alignment-Distortion in Packaging of Butterfly Laser Diode Modules: Simulation and Experiment

Yaomin Lin, *Student Member, IEEE*, Chad Eichele, and Frank G. Shi, *Member, IEEE*

***Abstract*—Controlling welding-induced-alignment-distortion (WIAD) and maintaining coupling efficiency is obviously the most challenging issue in assembling of fiber-optic components using laser welding. WIAD is the dominant barrier to having high packaging yields. Previous investigation has revealed that the WIAD in butterfly laser diode module packaging could be mitigated by properly choosing weld process parameters such as welding sequence. In this paper, the effect of welding sequence on WIAD is studied numerically by finite-element method (FEM) with a more realistic physics based laser welding model and experimentally by welding prototype butterfly packages. Results from both methods are compared. It is shown that the influence of welding process parameters on WIAD is significant and WIAD control is possible if proper welding sequence is employed.**

***Index Terms*—Butterfly laser diode package, fiber optic component attachment, finite-element method (FEM), laser welding, packaging yield, welding-induced-alignment-distortion (WIAD), welding sequence.**

I. Introduction

With rapidly increasing market demand for access to the information and the use of fiber optic communication technologies, the challenge in optical communications is to provide stable and high coupling efficiency photonic devices in high yield, mass quantities at lower costs. Laser welding technology has effectively being employed in the assembly of various photonic devices. As an alternative to common joining methods such as adhesive bonding and soldering, laser welding offers some attractive features such as submicron accuracy, strength, cleanliness, and long-term reliability [1]–[5]. Since its inherent advantages and proven performance, more and more communication system integrators are requesting laser welded packages from their suppliers.

To couple the light optimally from a laser diode into the fiber, welded parts must be able to hold the end of either a tiny fiber or waveguide with submicron precision. When laser welding is used to attach the laser diode module packages, it is necessary to have mechanical components such as metallic platform, ferrule, and weld clip to facilitate fiber handling and retention within the package. In the process of laser welding, it is expected that the rapid solidification of the welded parts and the associated material shrinkage lead to a relative movement between the pre-aligned components. The light coupling efficiency is reduced significantly by such a welding-induced-alignment-distortion (WIAD) or post-weld-shift (PWS). Effectively controlling WIAD to maintain high coupling efficiency is obviously the most challenging issue in assembling of fiber-optic components using laser welding.

WIAD or PWS has becoming an area of growing interest to researchers [6]–[11], and finite-element method (FEM) has been employed to predict or at least estimate the amount of WIAD that will occur. The factors that influence WIAD are various. They could be the laser parameters, the welding process parameters, the tooling geometries and properties of materials that involved. Our previous investigation has revealed that minimization of WIAD is possible in packaging of a laser diode module if relevant laser welding process parameters such as welding sequence can be optimized [9]–[11]. In finite-element modeling of the laser-material interaction, two pairs of welds (a front pair and a rear pair for a total of four) were placed in three different sequences. In the first sequence, the front welds and rear welds being placed simultaneously. The second sequence had the front welds placed first followed by the rear welds. The third sequence had the rear welds placed first followed by the front welds. The results showed that the least WIAD occurred when the front weld was placed first.

For simplicity, the laser intensity and laser energy absorptivity of material were considered as constants in our previous models. While qualitatively the results may remain correct for the optimal welding sequence, quantitatively the WIAD prediction may not have adequate accuracy, thus requiring further investigation.

In this paper, we investigate the effect of welding sequence on WIAD in butterfly packages with a more realistic physics based laser-welding numerical finite-element model and the experiment by welding prototype butterfly packages. The finite-element model deals with the welding cycles as an unstable coupled thermal stress problem with heat source, and it also introduces the spatial and temporal properties of welding lasers, nonlinear laser-material interactions, etc. The experiment was run on a laser weld workstation from Newport Corporation (Laser-

Manuscript received June 9, 2004; revised November 21, 2004.

Y. Lin and F. G. Shi are with the OptoElectronic Integration and Packaging Lab, University of California, Irvine, CA 92697 USA (e-mail: YAOMINL@uci.edu).

C. Eichele is with the Fiber Optic Division, ITT-Cannon, Santa Ana, CA 92705 USA.

Digital Object Identifier 10.1109/JLT.2004.841780

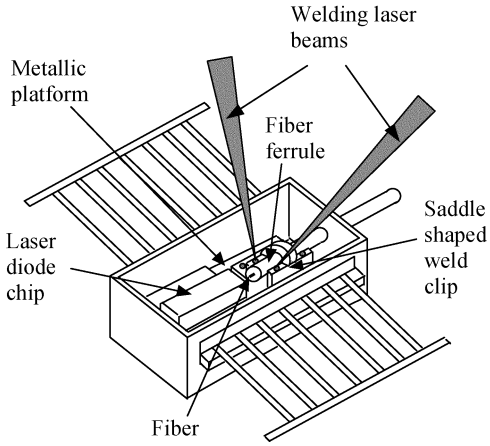

Fig. 1. Typical structure of butterfly laser diode module package with incident welding laser beams applied.

Weld Model LW4200), and it used the method of looking at the final alignment power of package for quantifying the net shift of the fiber. A comparison between the experimental results and the finite-element modeling predictions was made and it demonstrates that experiment results validated the FEM prediction both qualitatively in the way welding sequence affects WIAD and quantitatively in the magnitude of WIAD. The effect of welding sequence is shown to be significant on WIAD in butterfly laser diode packages.

The rest of the paper is organized as follows: the butterfly package structure, laser welding system and process are described in Section II. The basic equations and laser welding process modeling in finite-element analysis (FEA) are introduced in Section III. The FEA implementation and results are presented in Section IV. The experiment setup, process, the method for quantifying WIAD, and the results are described in Section V. The discussions and conclusions are drawn in Section VI.

II. Butterfly Laser Diode Module Package Structure, Laser Welding System, and Process

A. Butterfly Laser Diode Module Package Structure

A 980-nm laser diode module typically is composed of an optical subassembly (OSA) attached on a thermoelectric cooler in a 14-pin butterfly package (Fig. 1). The OSA is the platform onto which the laser diode, photodiode and some of the other components are mounted. It also includes a relatively large metallic platform onto which all the fiber pigtailing components are welded. Near the tip of a small length of the optical fiber is metalized and encapsulated in a cylindrical metallic fiber ferrule. After optical alignment of the fiber to the laser diode, the fiber ferrule is laser welded to a saddle shaped weld clip which is prewelded onto the metallic platform. The fiber ferrule, weld clip and the metallic platform are made of the same material so that their response to the weld induced stresses and strains are consistent and the stresses and strains within the assembled package are minimized.

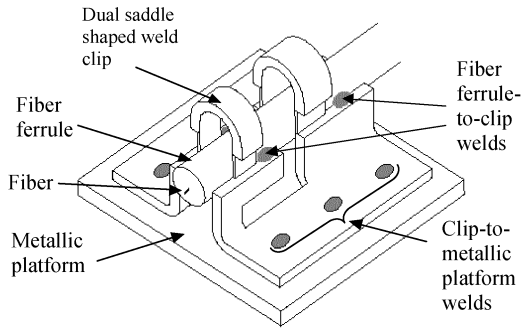

Fig. 2. Optical fiber is bonded onto the optical subassembly by welding of ferrule-to-clip and clip-to-metallic platform.

B. Laser Welding System & Process

The process of aligning and then attaching the optical fiber to the butterfly laser diode, which is referred to as fiber pigtailing, is conducted on LaserWeld Model LW4200 Workstation. The welding system is composed of a compact Nd:YAG laser, a laser beam delivery system, a fiber gripper mechanism, alignment stage with submicron accuracy, and laser weld process control software (PCS) which controls all associated devices (such as the stage clusters, laser diode modular controller etc.) and contains the interface for executing algorithms and writing sequences.

Weld spots are placed symmetrically with respect to the optical fiber axis. With this placement, the movement effects caused by laser welding in the lateral direction are cancelled out when welding simultaneously with multiple beams of equal intensity from opposing directions. But typically some net shift exists in the vertical direction. This shift (displacement) can be eliminated or minimized through optimal design of welding laser parameters and laser welding process.

In general, the laser welding of saddle shaped weld clip-to-metallic platform is implemented before welding of the fiber ferrule-to-clip. The relative movement in the package induced by welding of clip-to-metallic platform may be removed by realigning the optical fiber and laser diode after this welding. The relative movement in the package induced by welding of the fiber ferrule-to-clip directly results in the misalignment in the package. Therefore, in this research the WIAD by fiber ferrule-to-clip is of great interest. Fig. 2 depicts how the optical fiber is attached onto the OSA: the dual saddle shaped weld clip is first welded onto the metallic platform (with six weld spots totally), and then the fiber ferrule encapsulates the optical fiber is welded with the dual saddle shaped weld clip (with two pairs of weld spot: one pair that are near the laser diode chip are called front welds, the other pair are called rear welds).

The welding of the fiber ferrule-to-saddle shaped weld clip may be done by a different welding process. Three laser welding sequences are considered in the simulation effort of this research. The first case is the front and rear welds are made simultaneously. In the second case, the front welds are implemented at first, followed by the welding of the rear welds. In the last case, the welding sequence in the second case is reversed as that the rear welds are made at first, followed by the welding of the

front welds. The effect of the laser welding sequence on WIAD is investigated numerically by FEA.

III. Basic Equations and Laser Welding Process Modeling

A. Basic Governing Equations and Boundary Conditions

During the laser welding process, the thermal stress fields are produced by the nonuniform temperature distribution, the workpiece experience a nonsymmetrical cooling, the welds undergo a significant resolidification during cooling. The high intensity local heating of welding objects results in complex thermal strains and stresses, which finally lead to large residual stresses and small distortions. The process of laser welding is considered as a thermal/mechanical coupled process with heat source. The basic governing equations and boundary conditions are briefly introduced.

The spatial and temporal temperature distribution $T(x, y, z, t)$ for three-dimensional (3-D) heat conduction in a domain D satisfies the following differential equation

$$\rho c_p \dot{T} = \frac{\partial}{\partial x}\left(k_x \frac{\partial T}{\partial x}\right) + \frac{\partial}{\partial y}\left(k_y \frac{\partial T}{\partial y}\right) + \frac{\partial}{\partial z}\left(k_z \frac{\partial T}{\partial z}\right) + \dot{Q} \tag{1}$$

where ρ is mass density, c_p denotes specific heat capacity, T refers to temperature,k_{x}, k_{y}, k_{z}, refer to thermal conductivity in the x, y, and z directions, respectively, Q is heat generation per unit volume in the domain D, and the dot denotes derivative with respect to time. The initial condition is

$$T(x, y, z, 0) = T_0(x, y, z) \quad for\ (x, y, z) \in D \tag{2}$$

with the temperature field T_0 is a specified function of spatial coordinates.

Specified boundary conditions are required in this analysis and are determined as follows. On the given temperature boundary,

$$T = \overline{T} \tag{3}$$

where $\overline{T}$ denotes temperature applied as boundary constraint. On the heat convection boundary with the given atmosphere temperature

$$kT_{,n} = -h(T - T_\infty) \tag{4}$$

where k refers to thermal conductivity, h denotes coefficient of heat convection, T_∞ is ambient temperature. On the welded boundary with given laser heat flux $\overline{q}$

$$kT_{,n} = -\overline{q}. \tag{5}$$

Phase change happens during the laser-materials interaction, so, latent heat is induced. And it is assumed that the latent heat is uniformly released in a temperature range between solidus and liquidus temperatures of the materials involved.

For displacement response of the package during laser welding process, the finite deformation with finite plastic strain is considered. The nonlinear strain-displacement definition is used

$$\varepsilon_{ij} = \frac{1}{2}(u_{i,j} + u_{j,i} + u_{k,i}u_{k,j}) \tag{6}$$

where ε_{ij} is strain tensor, u_i denotes displacement vector. The total structure strain in a thermal stress problem is composed of elastic, thermal, and plastic components as

$$\varepsilon_{ij}^{Tot} = \varepsilon_{ij}^{E} + \varepsilon_{ij}^{T} + \varepsilon_{ij}^{P} \tag{7}$$

where ε_{ij}^{E} is elastic strain, ε_{ij}^{T} denotes thermal strain, ε_{ij}^{P} refers to plastic strain. The elastic constitutive equations is taken as

$$\sigma_{ij} = L_{ijkl}\varepsilon_{kl} \tag{8}$$

where L_{ijkl} denotes stiffness tensor. The thermal strain is computed from the coefficient of thermal expansion, which is temperature-dependent

$$\varepsilon^T = \int_{T_0}^{T} \alpha(T)dT \tag{9}$$

where $\alpha(T)$ is the coefficient of thermal expansion. The plastic strain is governed by the flow rule as

$$\varepsilon_{ij}^{P} = \dot{\gamma}\frac{\partial \phi}{\partial \sigma_{ij}} \tag{10}$$

where $\dot{\gamma}$ is consistent plasticity parameter, ϕ denotes plastic yield function. In this paper, the Mises yield criterion is used as

$$\phi = s_{ij}s_{ij} - 2B^2 \tag{11}$$

where B refers to yield strength of the material, S_{ij} is the deviator of the Kirchhoff stress tensor, which is defined as

$$s_{ij} = \sigma_{ij} - s\delta_{ij} \tag{12}$$

$$s = \frac{1}{3}s_{ii} \tag{13}$$

with Kroneck function

$$\delta_{ij} = \begin{cases} 1 & when\ i = j \\ 0 & when\ i \neq j. \end{cases} \tag{14}$$

The stress field of the system should satisfy the following equilibrium equations

$$\sigma_{ji,j} + p_i = 0 \tag{15}$$

where σ_{ij} denotes stress tensor, p is volumetric force. The boundary conditions is expressed as

$$n_i\sigma_{ij} = \overline{t}_j \tag{16}$$

where n_i is component of the outward normal vector of the given force boundary. The given displacement boundary is expressed as

$$u_i = \overline{u}_i \tag{17}$$

where $\overline{u_i}$ denotes displacement applied as boundary constraint.

B. Laser Welding Process Modeling

Lasers are useful for welding because the beam can be focused to high power intensity. Because of material reflectivity and heat transfer into the air, only a part of the heat energy that laser beam has is transferred into the material. In laser spot welding, the heat transfer is influenced by many parameters that are coupled one another. Some of the parameters, such as thermophysical properties and reflectivity are determined by respective materials, some others, such as laser pulse shape and beam polarization are under the control of operator. The energy transfer from the laser beam to the welding joints was simulated by the heat flux.

Laser welding process has been studied by many researchers and various models have been developed to describe the heat transfer in the fusion zone [12]–[17]. However, these models either ignored the materials' temperature dependent properties such as absorptivity, by assuming it as a constant, or disregarded the temporal characteristic of the laser beam. A proper laser welding model should combine the property of spatial and temporal power intensity distribution of the laser beam and the material dependent variables such as the thermophysical properties and absorptivity.

In this paper, the heat flux $q(x,y,z,t)$ on the top surface of the welds is expressed as

$$q(x,y,z,t) = \frac{QA(T)}{S} g(x,y) b(z) p(t) \tag{18}$$

where Q is the laser power to be transferred into the joints, $A(T)$ denotes temperature dependent absorptivity of material, S refers to characterized spot area, t is time, $g(x,y)$ reflects spatial property of laser beam, $b(z)$ describes the attenuation in the depth direction which obeys the Beer-Lambert Law, $p(t)$ reflects temporal property of laser beam (pulse shape). The heat flux is applied along the z-direction.

The laser beam shape (spatial property) employed in laser processing could be Gaussian beam, rectangular beam and circular beam. For a Gaussian beam, the beam profile is written as

$$g(x,y) = \exp\left(-\frac{(x^2+y^2)}{w_0^2}\right) \tag{19}$$

where w_0 is characteristic length of the laser beam. The intensity of a rectangular laser beam is a constant over its cross section $F = 2w_x * 2w_y$, the profile is given by

$$g(x,y) = H\left(w_x^2 - x^2\right) H\left(w_y^2 - y^2\right) \tag{20}$$

where H is the Heaviside function with

$$H(x) = \begin{cases} 0 & (x < 0) \\ 1 & (x \geq 0) \end{cases} \tag{21}$$

for a circular beam with constant intensity over its cross section $F = \pi w^2$, the profile is expressed as

$$g(x,y) = H\left(1 - \frac{r}{w}\right) \tag{22}$$

where $r = \sqrt{x^2+y^2}$.

The expression of $p(t)$ which describes the temporal property of laser beam is different with varying laser pulse shapes [11]. In this study, the laser pulse shape is considered as a Gaussian profile. Fig. 3 shows the temporal characteristic of laser beam. For a laser with Gaussian temporal distribution with a short pulse duration of τ_{p}, the pulse profile is written as

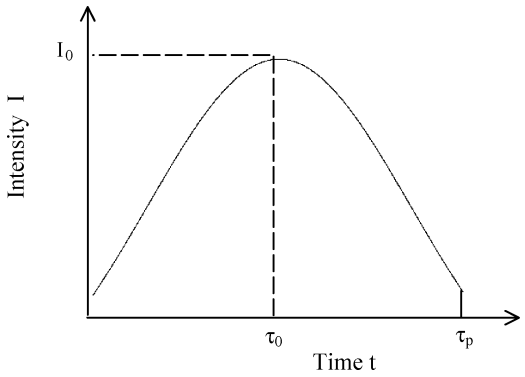

Fig. 3. Temporal property of laser beam—Gaussian pulse shape.

$$p(t) = \left(\frac{2}{\sqrt{\pi}\tau_p}\right) \exp\left(-\frac{4(t-\tau_0)^2}{\tau_p^2}\right) \tag{23}$$

where τ_0 is the time the maximum intensity is reached.

The material used for fiber ferrule, weld clip, and the metallic platform in the butterfly packages is Kovar. Material absorptivity of incident laser energy is not a constant, it changes with temperature: it is relatively small and increase slowly and linearly when temperature is low, when the temperature is increased above the materials' melting point, due to multireflection on the internal wall and plasma absorption, the absorptivity rises abruptly to a much higher value. Materials properties such as Young's modulus, yield stress, coefficient of thermal expansion, thermal conductivity, and specific heat are considered to be temperature dependent [10], [11].

IV. FEA

A. FEA Model

Fig. 4 gives the geometry of the dual saddle shaped weld clip and the local fiber ferrule structure. In the FEA, commercial software package of MARC and MENTAT are employed [18]. Due to symmetry of the physical structure, only half of it is considered. Six-nodes and eight-nodes thermal/mechanical coupled elements are employed in different areas. Totally, there are 7715 elements with 9835 nodes. The FE discretization of the structure is shown in Fig. 5. User subroutines describing the spatial and temporal characteristics of laser beam (laser power intensity distribution) and thermophysical properties of materials are developed and incorporated in the finite-element model.

Laser peak power intensity applied on the weld spots is 9000 $\mathrm{W/mm^2}$. The pulse duration is 5 ms. The radius of the weld spot is 200 μm for circular laser beam and the weld spot area is 400 $\mu\mathrm{m} \times 400$ μm for rectangular laser beam. The boundary conditions are applied as follows: 1) due to symmetry, the displacements of the nodes on the symmetric plane are fixed in x-direction; 2) since the dual saddle shaped weld clip is actually fixed (welded) onto the metallic platform, the movements

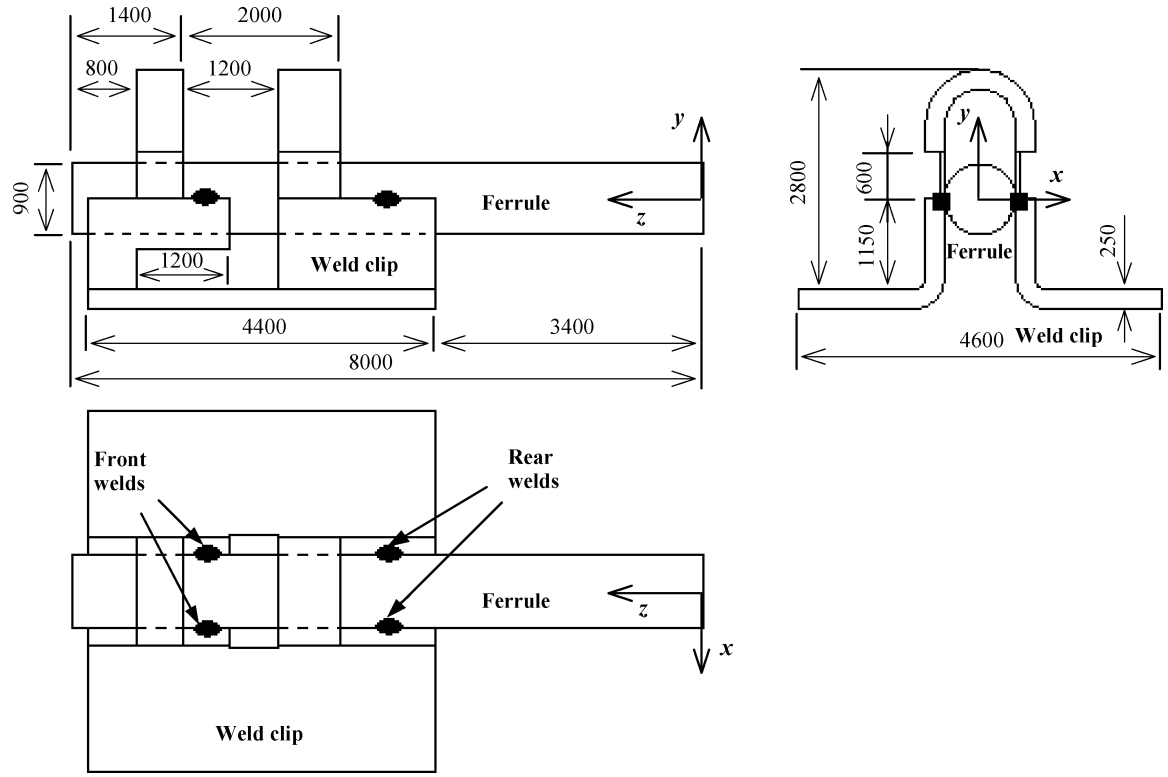

Fig. 4. Geometry of the dual saddle shaped weld clip and the local fiber ferrule structure (units: μm).

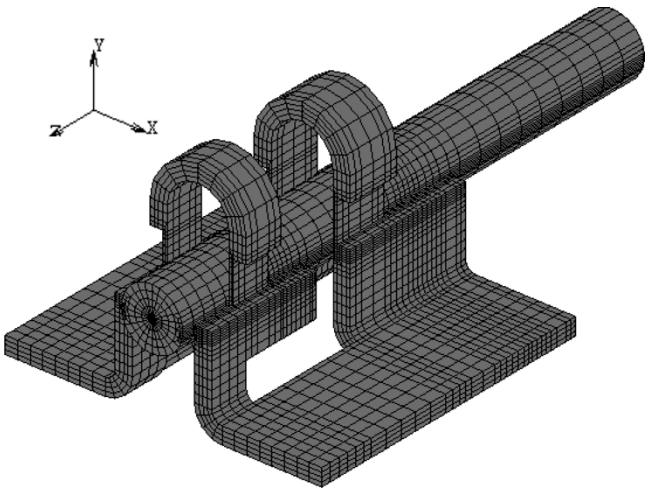

Fig. 5. FE discretization of the fiber ferrule-to-dual saddle shaped weld clip welding structure.

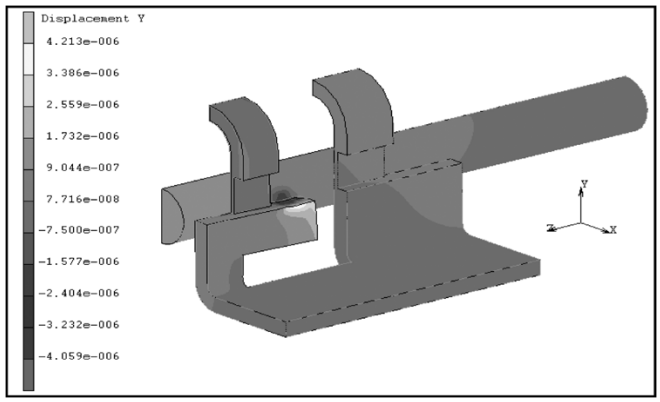

Fig. 6. Deformed shape of the model ($\times 5$) and the distribution of displacement (m) in y-direction after cooling of the front welding (circular beam and Gaussian pulse) for welding sequence case 2.

of the nodes located below the dual saddle shaped weld clip are constrained along all directions at the welding spots, the rest of the bottom surface of the weld clip is constrained along the vertical direction; 3) the movement of the nodes on the back end of the fiber ferrule is constrained before the cooling process begins (in real packaging process, the back end of the fiber ferrule is gripped by the pneumatic tweezers during welding implementation); 4) the interface between the surfaces of fiber ferrule and dual saddle shaped weld clip is constrained by no-penetration condition; 5) the heat flux which simulates the transferred laser beam energy is applied on the welding spots; 6) all rest of the surface is considered as heat convection with room temperature of 25 °C.

B. Results

The three cases of laser welding sequence considered in the investigation are: 1) the front and rear welds are made simultaneously, followed by cooling process up to the room temperature; 2) the front welds are implemented first, followed by cooling process in short time, then, the rear welds are made, followed by cooling process up to room temperature; 3) the rear welds are done first, followed by short time cooling, then, the front welds are implemented, followed by a cooling process up to room temperature.

Since the fiber center is located on the symmetric plane, the x-direction displacement is zero (realistically, the movement in the lateral direction is cancelled out by welding simultaneously with two beams of equal intensity from opposing directions).

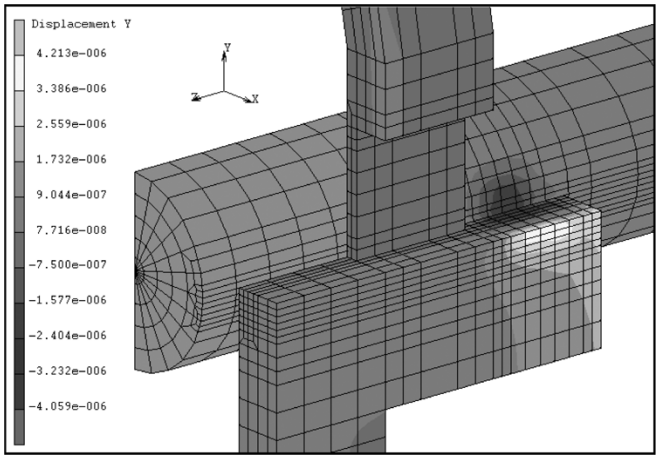

Fig. 7. Distribution of y-displacement (m) in vicinity of fiber tip and the front welds after cooling of the front welding (circular beam and Gaussian pulse) for the welding sequence case 2.

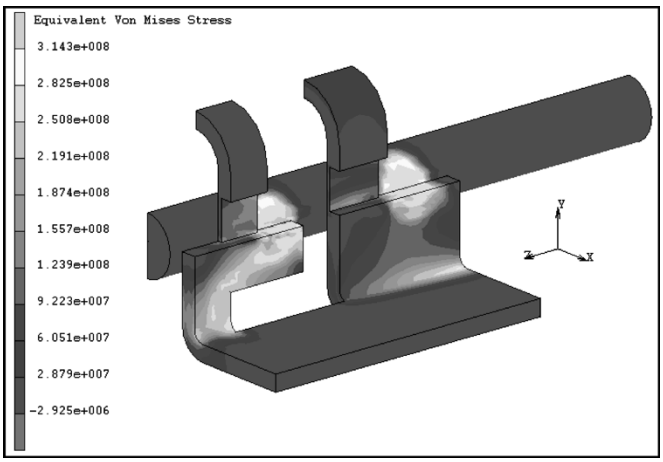

Fig. 8. Distribution of the von Mises stress $(\mathrm{N/m^2})$ after cooling process (circular laser beam and Gaussian pulse shape) for the welding sequence case 2.

TABLE I
THE WIAD INDUCED BY WELDING OF FIBER FERRULE-TO-DUAL SADDLE SHAPED WELD CLIP

Welding sequence / Beam properties / WIAD(μm)	Front & rear simultaneous	Front 1st and then rear	Rear 1st and then front
Circular beam	7.07	1.63	3.44
Rectangular beam	10.43	2.76	5.94
Gaussian beam	1.00	0.09	0.43
Average WIAD	6.17	1.49	3.27

On the other hand, the effect of displacement along the z-direction on the coupling loss is trivial. So, only the y-direction displacement of the fiber tip is of great concern. Fig. 6 shows the deformed shape ($\times 5$) of the model and the y-displacement distribution for welding sequence case 2. To be clear, the local distribution of the displacement in vicinity of fiber tip and the front welds is shown in Fig. 7. Fig. 8 gives the distribution of the residual von Mises stress after cooling process for welding sequence case 2.

Table I lists the displacements of the fiber center induced by laser welding for three welding sequences with different laser beam properties. The lasers are with a Gaussian temporal distribution. It is interesting to see that rectangular beam resulted in the largest distortion while this is understandable since rectangular beam has a larger surface to absorb the incident laser energy compared with other two beam shapes. Laser beam properties influence the rate of heat input into the material, and hence the WIAD. The effects of laser beam distribution on WIAD are averaged for the purpose of comparison to the experimental results.

V. EXPERIMENT

A. Experiment Setup and Process

Experiment procedure was developed to study the effect of welding sequence on WIAD. Ten butterfly laser diode module packages were assembled by joining the dual saddle shaped weld clip and fiber ferrule using YAG laser running on a LW4200 workstation. The dual saddle shaped weld clip and the fiber-ferrule are with the same dimension as those in FE model as described in earlier section. The material for the weld clip and fiber ferrule was Kovar.

The welding laser beam resembles a Gaussian distribution. The welding lasers were balanced for overall power and weld penetration. The two welding beams were set up 180 degrees from each other and 15 degrees off vertical. A 980-nm laser diode was placed into the "nest" of the LaserWeld such that current could be run through the device. A ferruled fiber was then prepped and loaded into the pneumatic grippers. One end of the fiber was spliced and placed inside an optical detector, which fed into an optical power meter, the other end was aligned to the laser diode. The current on the laser diode driver was set and the laser was turned on, then, alignment of the fiber to the laser diode began. Periodically, the initial alignment power was increased to determine whether the theory would hold for more delicate, higher power alignments. The 2-D profile was run and data was saved after alignment was achieved. The weld clip was then placed over the ferrule. The base welds that bonding the weld clip to the substrate were implemented. After realigning the fiber to the laser diode, the fiber ferrule was welded to the weld clip. Newport's PCS GUI was used to control all associated devices and execute all alignment scans including the 2-D profile.

A total of four welds were placed between the weld clip and fiber ferrule in pairs, two welds in the front (near the laser diode) and two in the rear. The power was recorded after each pair of ferrule welds was placed. Due to the configuration of the laser welding systems the scenario under which both pair of welds are placed simultaneously could not be tested. So, in this paper, the package was built using the welding sequence of cases 2 and 3. Five of the ten butterfly packages were built with the welding sequence case 2, i.e., the front welds made first, and the other five were assembled with the welding sequence case 3: rear welds implemented first. The position of the welds was referenced from the edge of the weld clip. Fig. 9 shows the base welds and the front ferrule welds. Fig. 10 gives the orientation of the front and rear ferrule welds with respect to the laser diode.

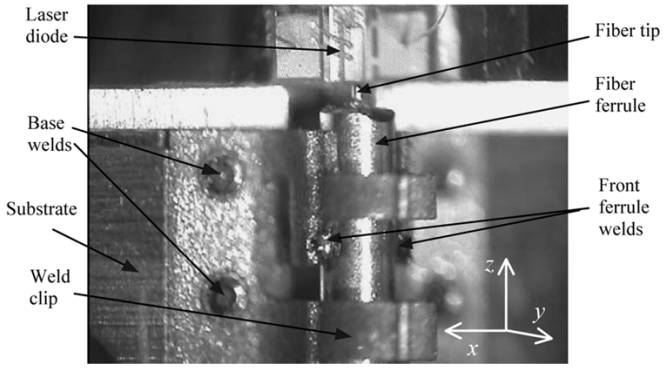

Fig. 9. Packages built during experiment with axis orientation.

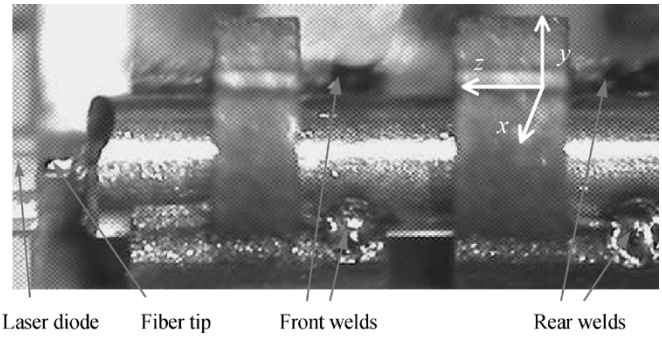

Fig. 10. Front and rear weld placement in relation to laser diode.

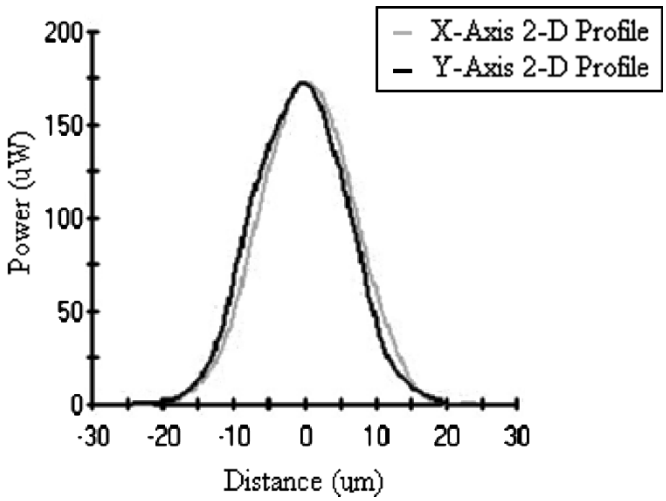

Fig. 11. *X* and *Y* axis 2-D profile graph centered on peak power.

B. Method for Quantifying WIAD

In reality, the package size is small and the shift is generally on the scale of microns, which make the determination of the WIAD a substantial challenge. There are however characteristics inherent in the laser weld process that may be used to track the WIAD with a certain degree of accuracy. Every shift away from alignment has some associated power loss. This relationship between shift and power loss can be mapped out via the 2-D profile as shown in Fig. 11. The data collected from the 2-D profile could be used to get an approximation of the magnitude of the total shift. It was assumed that shift that occurred outside the *y* axis could be neglected since the laser beams are well balanced. Net shift of the fiber tip was quantified indirectly by looking at final alignment power. The power lost due to the shift was then correlated back to the 2-D profile data to get a rough idea of the magnitude of the distortion. As an example, Table II gives the 2-D profile data for *y* axis relative position to the power (the data are not correlated to the profile graph in Fig. 11). We can see that if the power drops to 191.3 μW from 403.1 μW after the welds are placed then there has been a shift of approximately 5 μm.

Thus, the first piece of analysis will consist of determining which welding sequence resulted in the least power loss. This alone will tell us which sequence has less effect on the shift. Then the magnitude of the shift in each package built will be inferred by associating the power loss to the 2-D profile of that package at maximum power.

C. Results

Ten runs were made in the experiment with runs 1, 3, 5, 7, and 9 were with welding sequence case 2: front welding first followed by rear welding, and runs 2, 4, 6, 8, and 10 were with welding sequence case 3, i.e., rear welding first and then front welding. The results of the power loss in each run are listed in Table III. Because the initial power in each run was not always the same, the results are presented as percentages. The packages built with the front welds placed first (runs 1, 3, 5, 7, 9) had a much lower power loss than that with the sequence of with the rear welds placed first (runs 2, 4, 6, 8, 10).

This power data was then associated back to the 2-D profiles taken before welding began to yield an approximate net WIAD. The *y* axis 2-D profile data was used since with the welding laser beams balanced almost all shift occurs along the *y* axis. Table IV shows the WIAD associated with the power loss in the 10 runs.

The total power lost tended to increase as the initial power of the run was increased. This is because the higher power alignment has a more narrow power profile and thus it is more sensitive to the shift. It is interesting that the amount of shift correlated from the 2-D profile data is relatively consistent between runs of the same type (front weld first or rear weld first). This consistency gives more credence to the notion that the 2-D profile can be used to quantify WIAD.

VI. Discussion and Conclusion

The WIADs investigated from the experiment and predicted by the FE analysis are listed in Table V. There is a clear link between the welding sequence and the amount of WIAD that will occur. Experimentally, the final WIAD is 6.95 μm when the welding sequence is front welding first and then rear, and the WIAD is 19.3 μm when the welding sequence is rear welding first and then front. FEA shows that the final WIADs are 1.49, 3.27, 6.17 μm, respectively, when the welding sequences are front welding first and then rear, rear welding first and then front, and front and rear welds were made at the same time, respectively. In the experiment, due to some reasons the actual laser beams may not be absolutely balanced, this will bring in shifts outside the vertical direction. Therefore, the magnitude of the shift that is quantified by the method discussed is higher than

TABLE II
2-D PROFILE DATA FOR *Y* AXIS RELATIVE POSITION TO MAXIMUM POWER (403.1 μW)

Y-axis relative position (μm)	-5	-4.5	-4	-3.5	-3	-2.5	-2	-1.5	-1	-0.5	0
Power (μW)	191.3	219.2	248.6	277.6	304.2	329.9	353.5	372.6	387.8	399.3	403.1

TABLE III
DATA COMPARING ALTERNATE WELDING SEQUENCE

Front welds first	**Run 1**	**Run 3**	**Run 5**	**Run 7**	**Run 9**
Initial power (μW)	49.5	49.9	100.1	200.6	503
Power after front welds (μW)	41.8	41.7	91	102.9	127
Power after rear welds (μW)	44.1	46.7	98.1	145.7	222
Power loss (%)	11	6.5	2	27	56
Average power loss (%)	20.5				

Rear welds first	**Run 2**	**Run 4**	**Run 6**	**Run 8**	**Run 10**
Initial power (μW)	50.1	50.9	100.1	201.3	500
Power after rear welds (μW)	48.6	51.3	74.8	88	164
Power after front weld (μW)	37.3	44.2	19.5	7.7	1.12
Power loss (%)	26	12	80	96	99
Average power loss (%)	62.2				

TABLE IV
WIAD ASSOCIATED WITH POWER LOSS FROM 2-D PROFILE

Front welds first	**Run 1**	**Run 3**	**Run 5**	**Run 7**	**Run 9**
Total power lost (μW)	5.4	3.2	2	54.9	281
Shift from 2D profile data (μm)	12.5	5.5	2.5	7	7.25
Average WIAD (μm)	6.95				

Back welds first	**Run 2**	**Run 4**	**Run 6**	**Run 8**	**Run 10**
Total power lost (μW)	12.8	6.7	80.63	193.65	498.88
Shift from 2D profile data (μm)	18	17.5	22	21	18*
Average WIAD (μm)	19.3				

Notes: * This number had to be extrapolated from available data.

the FEA predictions. Nevertheless, the results from both experiment and FEA show that the significance of laser welding sequence on WIAD reduction is obvious: placing the front welds first at least reduced the WIAD by half than placing the rear welds first.

In photonic packaging using laser welding, the process of manipulating both the upward and downward movements of the fiber tip by varying the position and intensity of the spot welds is well known as "laser hammering." Normally at least two spots are required in order to join the fiber-optic components together. The newly formed welding spots tend to pull the fiber ferrule downwards. The previously formed welding spots act as a pivot at the time the sequent welding are performed. If the beam is directed toward the back of the weld clip, the downward distortion at the rear tends to pivot the front of the fiber upwards, like a balance (Fig. 12). The welding sequence case 2, i.e., the front welds made first and then rear, is exactly in accordance with this process. It is actually the vivid application of "laser hammering," thus the residual displacements in the assembly are compensated and minimized.

TABLE V
COMPARISON OF WIADS BY EXPERIMENT AND FEA (UNITS IN μm)

Welding sequence	Experiment	FE analysis
Front welds 1st and then rear welds	6.95	1.49
Rear welds 1st and then front welds	19.3	3.27
Front and rear welds simultaneous	N/A	6.17

Based on the above analysis by experiment and FEA, the following conclusions are obtained.

1) Laser welding sequence has a significant influence on the WIAD in butterfly laser diode module packages. Optimal selection of welding sequence can at least reduce the WIAD by half.
2) A more realistic physics based laser welding model is developed and incorporated in the finite-element model for WIAD prediction in butterfly packages. Qualitatively,

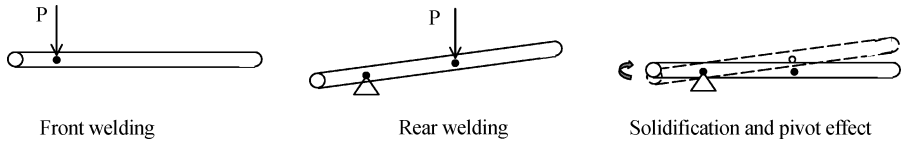

Fig. 12. Pivot effect in the welding sequence case 2.

good agreement is obtained between the FEA and the experimental results. The results show that the model is applicable and numerical method could provide guidelines to process design optimization.

3) Effect of other process parameters and tooling design parameters in laser welding on WIAD is not negligible. Their influence can be evaluated by means of numerical method to save design and product cost and time.

ACKNOWLEDGMENT

The LaserWeld Model LW4200 workstation at the OptoElectronic Integration and Packaging Laboratory of the University of California, Irvine, was donated by Newport Corporation. The authors are grateful for the support.

REFERENCES

[1] S. Jang, "Automation manufacturing systems technology for opto-electronic device packaging," in *Proc. 50th Electron. Comp. Technol. Conf.*, Las Vegas, NV, May 2000, pp. 10–14.

[2] R. Heyler, "Package design considerations for automated assembly," *Fiberoptic Product News*, Aug. 1999.

[3] G. Shannon and E. Palen, "Laser-weld attachment enables repeatable submicron precision," *Optoelectron. Manufact.*, vol. 1, no. 2, May 2002.

[4] C. Marley and M. Rodighiero, "Laser welding produces high-yield assembly and packaging," *Laser Focus World (Suppl. Issues)*, pp. 59–64, Aug. 2001.

[5] V. T. Kowalski, R. J. Coyle, P. P. Solan, and K. M. Hogan, "Laser weld process improvements for optical isolator assembly," in *Proc. 45th Electron. Comp. Technol. Conf.*, New York, 1995, pp. 1116–1121.

[6] W. K. Huang, Y. C. Hsu, M. T. Sheen, and W. H. Cheng, "Post-weld-shift in butterfly package," in *Proc. 4th Int. Symp. Electron. Materials and Packaging*, Piscataway, NJ, 2002, pp. 77–82.

[7] J.-H. Kuang, M.-T. Sheen, S.-C. Wang, G.-L. Wang, and W.-H. Cheng, "Post-weld-shift in dual-in-line laser package," *IEEE Trans. Adv. Packag.*, vol. 24, pp. 81–85, Feb. 2001.

[8] M. Labudovic and M. Burka, "Finite element analysis of post-weld shift during fiber pigtail of 980 nm pump lasers," *IEEE Trans. Adv. Packag.*, vol. 26, pp. 41–46, Feb. 2003.

[9] W. N. Liu, Y. M. Lin, and F. G. Shi, "Welding induced alignment distortion in DIP LD packages: effect of laser welding sequence," in *Proc. SPIE*, vol. 4652, San Jose, CA, 2002, pp. 128–135.

[10] Y. M. Lin, W. N. Liu, and F. G. Shi, "Laser welding induced alignment distortion in butterfly laser module packages: effect of welding sequence," *IEEE Trans. Adv. Packag.*, vol. 25, pp. 73–78, Feb. 2002.

[11] Y. M. Lin and F. G. Shi, "Effects of welding sequence on laser welding induced alignment distortion in butterfly laser diode module packages," in *Proc. SPIE*, vol. 4997, San Jose, CA, 2003, pp. 30–39.

[12] J. Mazumder and W. M. Steen, "Heat transfer model for CW laser material processing," *J. Appl. Phys.*, vol. 51, pp. 941–947, 1980.

[13] T. Zacharia, S. A. David, J. M. Vitek, and T. DebRoy, "Heat transfer during Nd:YAG pulsed laser welding and its effect on solidification structure of austenitic stainless steels," *Metallurgical Trans. A*, vol. 20A, pp. 957–967, May 1989.

[14] N. Sonti and M. F. Amateau, "Finite-element modeling of heat flow in deep-penetration laser welds in aluminum alloys," *Numerical Heat Transfer A*, vol. 16, pp. 351–370, 1989.

[15] O. O. Diniz Neto and C. A. S. Lima, "Nonlinear three-dimensional temperature profiles in pulsed laser heated solids," *J. Phys. D*, vol. 27, pp. 1795–1804, 1994.

[16] M. R. Frewin and D. A. Scott, "Finite element model of pulsed laser welding," *Welding J. Res. Suppl.*, vol. 78, pp. 15s–22s, Jan. 1999.

[17] W. S. Chang and S. J. Na, "A study on the prediction of the laser weld shape with varying heat source equations and the thermal distortion of a small structure in micro-joining," *J. Mater. Processing Technol.*, vol. 120, pp. 208–214, 2002.

[18] MSC.Software Corporation, MSC.MARC User's Guide, MSC.Software, Inc., 2001.

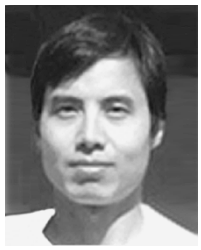

Yaomin Lin (S'03) received the M.S. degree in mechanical engineering from Beijing University of Technology, Beijing, China, in 1998, and is currently pursuing the Ph.D. degree in optoelectronic integration and packaging at the University of California, Irvine.

He is a Research Assistant with the OptoElectronic Integration and Packaging Lab, University of California, Irvine.

Chad Eichele received the B.S. degree in physics and the M.S. degree in engineering both from the University of California, Irvine.

He is currently with the Fiber Optic Division, ITT-Cannon, Santa Ana, CA, working as an engineer.

Frank G. Shi (M'01) received the Ph.D. degree from the California Institute of Technology, Pasadena, in 1992.

He is a professor and director of the OptoElectronic Integration and Packaging Lab, University of California, Irvine.